https://doi.org/10.5194/ar-2026-6
Preprint. Discussion started: 4 February 2026

Iberulite fall and formation mechanism during a Sahara dust event in Switzerland in February 2021

Bernard Grobety [1,3], Philippe Favreau [2], Juanita Rausch [1], David Jaramillo [1], Martin Steinbacher [4], Christoph Neururer [3]

[1]Particle Vision GmbH, Passage du Cardinal 13B, 1700 Fribourg, Switzerland;
bernard.grobety@unifr.ch, juanita.rausch@particle-vision.ch, david.jaramillo@particle-vision.ch
[2] Service de l'air, du bruit et des rayonnements non ionisants (SABRA), Geneva Cantonal Office for the Environment, 1205, Geneva, Switzerland ; philippe.favreau@etat.ge.ch
[3]Geoscience Department, University of Fribourg, Chemin du Musée 6, 1700, Fribourg, Switzerland;
christoph.neururer@unifr.ch
[4]Empa, Laboratory for Air Pollution and Environmental Technology, 8600 Duebendorf, Switzerland;Martin.Steinbacher@empa.ch

Correspondence to: Bernard Grobety (bernard.grobety@unifr.ch)

Abstract. Sahara dust events can promote the formation of micrometer-sized spherical mineral aggregates known as iberulites as they are usually found on the Iberian Peninsula. Iberulites have not, to our knowledge, been reported from Central Europe. Two formation mechanisms – in- and below-scavenging – have been proposed. Strong iberulite fall (IFs) were observed in Switzerland in February 2021 when large amounts of dust were transported from the Moroccan-Algerian border towards Central Europe during a Saharan Dust Event (SDE). In contrast to the previous IFs observed on the Iberian Peninsula, this IF occurred under low-temperature conditions e.g. near the freezing point in the cloud and at the surface. The relative humidity in the first 1000 m below the clouds decreased from 70 to 40%. and the comparison between particle-size distribution (PSD) within the iberulites and the dust PSD in the free atmosphere revealed a Greenfield gap in the iberulites, e.g., a lack of particles in the range 0.1-0.3µm relative to the dust in the free atmosphere. The meteorological conditions, the microstructure of the iberulites, and the presence of a Greenfield gap point to below-cloud scavenging as the most likely formation mechanism. Further discoveries of iberulite in Swiss SDE samples suggest that the phenomenon is widespread and not only limited to regions close to the dust source.

Deleted:
Deleted: below
Deleted: given
Deleted: Western

https://doi.org/10.5194/ar-2026-6
Preprint. Discussion started: 4 February 2026

1 Introduction

Sahara Dust Events (SDEs) occur approximately 10-40 times each year over the Alps, greatly increasing aerosol levels. They peak from February to June and October to November (Coen et al., 2004; Flentje et al., 2015; Mauro et al., 2019). Since 2020, SDEs in February and March have become more frequent, especially in the Western Euro-Mediterranean region (Cuevas-Agulló et al., 2024), leading to higher dust concentrations. This trend is driven by westerly wind blockages shifting poleward due to blocking highs and the development of cutoff subtropical lows. During these events, aerosol levels often exceed European, Swiss, and WHO PM10 standards (24-hour limit: 50 µg/m³ (European, Swiss), 45 µg/m³ (WHO); during events: 55 µg/m³), with ground-level concentrations during the SDEs exceeding the limits by a factor of 2. Desert dust has been associated with adverse health effects, including increased cardiovascular mortality and respiratory issues, although impacts vary by the dust's geographic source (Fussell and Kelly, 2021; Tobias et al., 2019). In Europe, dust accounts for over 40,000 deaths annually (Wang et al., 2020). To date, 150 countries are affected, with more than 100 classified as non-dust-source regions (Li et al., 2025). Due to the growing threat of sand and dust storms, international agencies have prioritized mitigation efforts over the past twenty years (Uncod, 2022). Dust also influences climate and ecosystems (Buseck and Pósfai, 1999; Lian et al., 2025) by affecting Earth's radiative balance (Heald et al., 2014), degrading air quality (Proestakis et al., 2025), supplying nutrients to marine and terrestrial ecosystems (Kellogg and Griffin, 2006), reducing snow and ice albedo to accelerate melting (Francis et al., 2018), and adsorbing trace gases, altering their physical properties (Tan et al., 2024). Saharan dust notably impacts hail formation in Europe (Brennan and Wilhelm, 2025). Limited research exists on the economic impact of desert dust, and no standardized data collection or analysis (Middleton, 2017). Annual dust-related damages in Iraq and Iran are estimated between $1.0 billion and $1.4 billion (Meibodi et al., 2015). In the U.S., costs related to dust and wind erosion reached $154 billion in 2017, more than quadrupling since 1995 (Feng et al., 2025).

A distinct type of dust particles are spherule-shaped aggregates measuring between 50 and 200 µm, called iberulites, a term originating from their first discovery in southern Spain (Díaz-Hernández & Párraga, 2008). Iberulites have also been identified in Mallorca (Fiol et al., 2005; Fiol & Guijarro, 2000) and in Tenerife (Spain) (Cuadros et al., 2015), but no sightings have been reported north of 42°N. Iberulites found in Spain display flow textures, including typical depressions (vortices) and a shell structure with a coarse-grained core and a dense, fine-grained surface layer (Díaz-Hernández & Párraga, 2008; Párraga et al., 2021). They contain minerals such as silicates, carbonates, sulfates, halides, oxides, and phosphate-vanadates, along with plant material, silica shells, plankton, and probably viruses. This mineral composition suggests the Sahara and Sahel as primary mineral sources, while other minerals such as gypsum and alunite-jarosite are likely formed in the atmosphere (neoformation), probably via atmospheric pollutants during transport (Díaz-Hernández & Párraga, 2008; Párraga et al., 2021).

Two mechanisms are proposed for creating these aggregates (Díaz-Hernández & Sanchez-Navas, 2016; Párraga et al., 2021):

1. Coalescence of droplets within a cloud increases condensation nuclei within a single droplet, known as in-cloud scavenging

https://doi.org/10.5194/ar-2026-6
Preprint. Discussion started: 4 February 2026

(ICS) or 'nucleation scavenging,' and 2. increase in concentration through collisions between particles and falling drops, called below-cloud scavenging (BCS) or impaction scavenging (Pruppacher & Klett, 2010). The efficiency of a drop in coalescing or collecting particles is called Number Scavenging Efficiency (NSE) for ICS (Yang et al., 2023), and collection efficiency (CE) for BCS (Laakso et al., 2003; Slinn, 1977, 1983; Volken & Schumann, 1993). If CE were. unaffected by factors such as drop and particle properties or environmental conditions, the grain-size distribution in iberulite would match the dust-size distribution in the cloud (ICS) or the volume of air passing through (BCS). However, ICS depends on aerosol activation, influenced by particle size, composition, coatings, and atmospheric water saturation. Dust particles with soluble coatings are highly effective cloud condensation nuclei (CCN) (Levin et al., 2005). Small amounts of soluble material greatly increase the CCN activity of fine dust particles (Kelly et al., 2007). Larger dust particles can act as giant CCN, forming efficient collector drops (Feingold et al., 1999; Levin & Cotton, 2009). Recent evidence shows insoluble species, such as freshly emitted mineral dust, can also serve as CCNs, even with little soluble material, especially if they contain soluble ions or have strong water vapor adsorption on their surfaces (Herich et al., 2009; Koehler et al., 2009; Kumar et al., 2009). Mineral dust's contribution to CCN levels decreases at lower supersaturations because insoluble aerosols are less hygroscopic and need higher supersaturation to activate compared to soluble particles. Nonetheless, since dust particles are coarser, coated particles can activate at lower supersaturations than smaller human-made aerosols. At 0.2% supersaturation, mineral dust accounts for up to 30% of CCN, increasing to 35% at 0.4%. NSE, or water adsorption efficiency, varies with particle type, size, and supersaturation. For dust particles between 0.3 and 1 µm, NSE remains around 0.2 (Yang et al., 2023). For particles larger than 1.0 µm, NSE increases, whereas particles between 0.1 and 0.3 µm are often removed by impaction, reducing NSE to about 0.1. For BCS, the capture efficiency depends on particle size and the capture mechanism. If the drop with a radius R falls vertically, e.g., no deviation by wind, the maximum number of possible collisions N along a trajectory l within the dust layer with particle radius r, mass density Md, and particle density d can be calculated.

$$N = \frac{3}{4}\frac{2\pi M_d R^2 l}{\pi r^3 d} \quad (1)$$

For particles larger than 1 µm in diameter colliding head-on with a droplet, bouncing is unlikely, and the sticking efficiency is assumed to be 100%. However, for particles with radii between 0.3 µm and 1 µm, the CE, which is defined as the ratio of the total number of collisions given by eq. 1 to the number of particles captured by the droplet, is less than 1. This occurs because of the airflow around the falling droplet. Particles in this size range, although on collision trajectories, tend to follow the flow lines and are diverted around the droplet. Larger particles, due to their inertia, cross the flow lines and impact the droplet directly, resulting in a CE of 1 (capture by impaction). Small particles (< 0.3 µm) that follow the flow lines may be pushed by Brownian motion into the droplet's wake and deposited on its rear end (Brownian capture), making the CE also close to 1. Capture can also occur through thermophoretic and diffusiophoretic forces. Thermophoretic forces push aerosol particles toward a frozen drop during evaporation and away from it during vapor deposition. During diffusive crystal growth, a flow known as Stefan's flow exists near the hydrometeor surface, exerting a force on nearby aerosol particles that pulls them toward the surface. Particles, regardless of their size, can follow flow lines, but at some point, these lines get closer to the

https://doi.org/10.5194/ar-2026-6
Preprint. Discussion started: 4 February 2026

droplet's surface than the particle's radius. The particle then contacts the droplet's surface and sticks to it (capture by interception). This process has a relatively low capture efficiency. For particles with radii between 0.3 and 1.0 µm, none of the preferred capture processes are effective, and the CE decreases by two orders of magnitude. This reduction in CE was first described by Greenfield (1957), and the absence of particles in the 0.3–1.0 µm range is called the Greenfield gap. Both formation mechanisms lead to a depletion of particles in the 0.3–1.0 µm range in the iberulites relative to the dust cloud concentration, but the decrease is much more pronounced for BCS. The particle size distribution (PSD) inside an iberulite, compared to the PSD in the free atmosphere, can therefore indicate the formation mechanism of the iberulite.

Dust from potential source areas has been characterized by bulk chemistry and mineralogy (Kandler et al., 2007; Scheuvens et al., 2013). Mineralogical fingerprints include phyllosilicates, such as the ratio of illite to kaolinite concentrations (I/K) (Caquineau et al., 1998; Chester and Johnson, 1971; Scheuvens et al., 2013). The general trends in Northern Africa show increases in I/K from south to north and from east to west. High carbonate contents (>10 wt.%, calcite > dolomite) also serve as a fingerprint of dust from northwestern Africa (Avila et al., 1997). Similar to illite, carbonate content decreases steadily toward the south (Paquet, 1984). The high carbonate content of dust emitted from the northern regions within and near the Atlas Mountains reflects the geology of those areas (Grousset et al., 1992).

A major SDE struck Switzerland on the afternoon of February 6th, 2021, making it one of the strongest since systematic monitoring began in 2001 (Collaud Coen et al., 2025) at the Jungfraujoch laboratory (JFJ, inlet altitude 3585 m above sea level). Due to its elevation and low local emissions, JFJ is ideal for studying long-range transport processes. A record PM10 concentration exceeding 700 µg/m³ was recorded (NABEL, BAFU/Empa). The iberulite fall (IF) was observed by the authors in Saint-Légier (Vaud), Fribourg (Fribourg), and Geneva. This study aims to characterize the collected iberulites and examine the aggregation mechanism in detail, using well-documented meteorological conditions during the fall.

Commented [JR1]: Probably not only in those locations. But observed by us. Therefore, I suggest to add "by the authors"

Deleted: <#>Sahara Dust Events (SDEs) reach about 10-40 t
and significantly contribute to the aerosol¶
load above the region, with strongest influence from February
November (Coen et al., 2004; Collaud¶
Coen et al., 2025; Mauro et al., 2019; Flentje et al., 2015). SD
particularly increased since 2020¶
(Cuevas-Agulló et al., 2024). Aerosol concentrations during t
European and Swiss air quality¶
standards and the WHO PM10 air quality guidelines. There is
human health, e.g., increases¶
in cardiovascular mortality and respiratory morbidity, but the
when considering the dust's¶
geographical origin (Fussell and Kelly, 2021; Tobias et al., 20
ecosystems (Buseck and¶
Pósfai, 1999; Parajuli et al., 2022). Although the importance
mineralogical studies are scarce¶
(Engelbrecht and Derbyshire, 2010).¶
A special form of dust aerosol particles are giant spherule-sha
200 µm in diameter. These¶
"microspherulites" are called iberulites, in reference to their f
(Díaz-Hernández and Párraga,¶
2008). Such iberulites were also reported from Mallorca (Spa
Tenerife (Spain) (Cuadros et al.,¶
2015), but no observations have been reported from regions N
are thought to form inside¶
raindrops by the coalescence of smaller droplets in a cloud, th
condensation nuclei in the latter,¶
or by the capture of particles below a cloud by drops as they f
Hernández and Párraga, 2008). A major¶
SDE hit Switzerland at the beginning of February 2021. Syste
conducted in Switzerland at the¶
Jungfraujoch Sphinx observatory (inlet altitude 3585 m above
2020)) since 2001 (Collaud Coen¶
et al., 2025). Due to its elevation and the negligible local emis
location to investigate long-¶
range transport processes (Herrmann et al., 2015). The event
one of the strongest SDEs since¶
its systematic monitoring in 2001 (Collaud Coen et al., 2025).
February 6th, 2021in the afternoon.¶
At Jungfraujoch, a record PM10 concentration of more than 7
(NABEL, BAFU/Empa). The IF¶
analyzed here happened at lower altitudes in the village of Sa
46.471° N, 6.877°E), the city of¶
Fribourg (canton of Fribourg, 46.717° N 7.083° E), and the ci
46.033° N, 6.117° E), all in¶
western Switzerland. Until now, two formation processes of i
and below-cloud scavenging.¶
The goal of the present work is to explore the aggregation me
leveraging the well-documented¶
meteorological conditions during the fall in our case.¶

https://doi.org/10.5194/ar-2026-6
Preprint. Discussion started: 4 February 2026

2 Methods

2.1 Iberulite collection

The fall of the Iberulites was observed in the early afternoon of February 6th in St. Légier (46.471° N, 6.877° E), Fribourg (46.717° N, 7.083° E), and Geneva (46.204° N, 6.143° E) (Fig. 1, Table 1). Iberulites were collected in all three sites. The city of Fribourg (500-700 m ASL)) is 50 km NNE of Lake Geneva on the Swiss plateau, and the village of St. Légier (576 m ASL) is on the central northern shore of the same lake. The geology of the surroundings of both sites is dominated by calcareous mountains (Jura, Préalpes) (Jones et al., 2024). Loss of particles during dispersal on the foil is negligible.

Collecting dust on aluminum foil is not a common method, but since the IF was unexpected, standard sampling equipment, such as a sampling head with an impactor and a pump, could not be set up in time. Aluminum foils are used to collect interstellar dust (Kearsley et al., 2010) and to identify laboratory sources of microplastic and nanoplastic contamination (Jones et al., 2024). Loss of particles during dispersal on the foil is negligible.

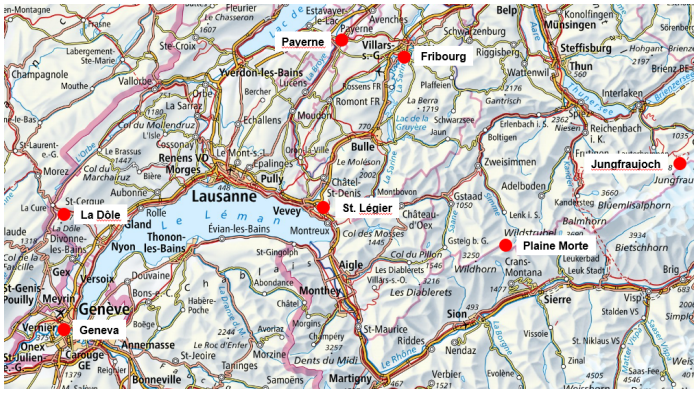

Figure 1: Locations in Western Switzerland mentioned in the text (Swisstopo, 2025).

Table 1 Sampling sites and analyses done (iber.: iberulite; opt.: binocular imaging)

Site	Sampling	Dust PSD	Iber. PSD	Dust XRD	Dust SEM	Iber. Opt.	Meteo
Fribourg							
St. Légier							
Genève							
Jungfraujoch							
Payerne							

Deleted: Collection sites¶
Deleted: on
Deleted: from all three sites
Deleted: St. Légier, Fribourg, and Geneva¶ (Switzerland).
Deleted: ¶
Deleted: dominated by calcareous mountains (Jura, Préalpes) 2011). In St.Légier, the iberulites were¶ picked up from the ground with tweezers, and in Fribourg, an ground, from which samples were¶ collected with a fine spatula. The iberulites were gently deposi head specimen mounts and¶ boron substrates (see below).
Deleted: <#>The high-Alpine station Jungfraujoch (7.98° N, 4 northern Swiss Alps. Its remote location,¶ far from local anthropogenic sources, makes it ideally suited f atmospheric conditions over central¶ Europe. Jungfraujoch hosts a comprehensive long-term in-situ and trace gas as a contribution¶ to the Global Atmosphere Watch (GAW) program of the Worl (WMO) (Bukowiecki et al.,¶ 2016) and is part of the Swiss National Air Pollution Monitori
Deleted: .
Deleted: .

https://doi.org/10.5194/ar-2026-6
Preprint. Discussion started: 4 February 2026

2.1 Meteorological data

Meteorological data were obtained from radio sounding balloons, which are launched by the Federal Office for Meteorology and Climatology of Switzerland (MeteoSwiss) station in Payerne (46.817° N, 6.933° E), twice a day (23:00 and 11:00 h UTC). Payerne is located 17 km west and 47 km north of the collection sites in Fribourg and St. Légier, respectively. The station is equipped with a Raman lidar, ceilometers, and a Doppler radar to measure precipitation, aerosol concentration, and wind profiles. On February 6th, the ceilometer profile series from Payerne exhibited gaps in the morning and smaller ones in the afternoon due to ground fog. The area is also covered by two weather radars: one on La Dole Mountain (46.425°N, 6.099°E), west of St. Légier and near Geneva, and the other on the Plaine Morte (46.383°N, 7.500°E), in the central Bernese Alps southeast of the two collection sites.

The size distributions of fine- and coarse-mode aerosols in the dust cloud were measured at the high-altitude Alpine station Jungfraujoch (JFJ, 7.98° N, 46.55° E; 3580 m ASL, Fig. 1), located in the Bernese Alps. Its remote location, far from local human sources, makes it ideal for monitoring background atmospheric conditions over central Europe. Jungfraujoch hosts a comprehensive long-term in situ monitoring program for aerosols and trace gases as part of the Global Atmosphere Watch (GAW) program of the World Meteorological Organization (WMO) (Bukowiecki et al., 2016), and is included in the Swiss National Air Pollution Monitoring Network (Hüglin, 2021). Aerosol measurements have been conducted using a custom-built Scanning Mobility Particle Size Spectrometer (SMPS) (Wiedensohler et al., 2012; Jurányi et al., 2011) and a white-light optical particle size spectrometer (FIDAS, Palas GmbH, Germany)(Brem et al., 2023)(Fischer and Hüglin, 2024).

2.3 Dust trajectory analysis

The dust RGB product, based on three infrared channels of the Spinning Enhanced Visible and InfraRed Imager (SEVIRI) on EUMETSAT's MSG-11 satellite (Schmetz et al., 2002), was used to to identify the sources of afternoon dust arriving over western Switzerland (Schepanski et al., 2009). The dust detection method relies on the brightness temperature differences at 12.0 μm minus 10.8 μm and 10.8 μm minus 8.7 μm, as well as at 10.8 μm (Sokolik, 2002). The plume's path was tracked using satellite images following the approach described by (Ashpole and Washington, 2013). The visually determined dust trajectories were verified by both forward and backward trajectory calculations using the Hybrid-Single Particle Lagrangian Integrated Trajectory (HYSPLIT) model developed by the National Oceanic and Atmospheric Administration's (NOAA) Air Resources Laboratory (ARL) (Draxler and Rolph, 2003).

Deleted: The size distributions of fine-mode and coarse-mode measured by a home-built Scanning Mobility¶
Particle Size Spectrometer (SMPS) (Wiedensohler et al., 2012 white-light optical particle size¶

Deleted: <#>spectrometer (FIDAS, Palas GmbH, Germany) (respectively.¶

Deleted: (https://www.eumetsat.int/0-degree-service),

Deleted: determine the origin of the dust¶
arriving in the afternoon over western Switzerland. The plume

Deleted: traced on satellite images using the approach¶

Deleted: ¶

Moved (insertion) [1]

Deleted: ¶

Deleted: ¶

https://doi.org/10.5194/ar-2026-6
Preprint. Discussion started: 4 February 2026

HYSPLIT uses archived 3-dimensional meteorological fields generated from ground and satellite observations, as well as short-term forecasts. or this study, the Global Forecast System dataset from the National Centers for Environmental Prediction at a 0.25° resolution was employed for back-trajectory calculations. The SERVIRI images and the backward trajectories trace the dust's origin for an arriving time over Fribourg at 2000 meters above ground level (AGL), between 12:00 and 18:00 UTC on February 6, roughly coinciding with the period of highest cloud density) to the Algerian - Morrocan border. The dust source meteorological data were obtained via the Real-time Environmental Applications and Display sYstem (READY) from the archived Global Data Assimilation System (GDAS) (Rolph et al., 2017). The data were obtained for the center of the primary dust source observed in the satellite image, e.g., 33.8°N, 1.5°W.

2.4 Scanning Electron Microscopy (SEM) and Optical Polarization Microscopy (OPM) analyses

Single particles and iberulites were isolated from samples collected on the ground in St. Legier and Geneva, as well as on an aluminum foil in Fribourg. A selection of iberulites was gently placed onto a ½" pin stub mount (Ted Pella, Redding, CA, USA) and examined using an Olympus SZX12 binocular microscope (Tokyo, Japan). All single particles collected on the foil in Fribourg were dispersed onto a carbon pad covered 1-inch pin stub and analyzed using automated SEM/EDX single-particle analysis (Computer-Controlled SEM, CCSEM). During CCSEM, particles are identified based on their Back-Scattered Electron (BSE) contrast, and images, along with Energy-Dispersive X-ray (EDX) spectra, are acquired. For this, a FEI Sirion FEG microscope equipped with an Oxford X-MAX EDX detector with a 150 mm^2 sensor size, a four-quadrant BSE detector, and AZtecFeature software (Oxford Instruments) was used at the Department of Geoscience of the University of Fribourg (Fribourg, Switzerland). The analyses were performed at 20 kV. EDX analyses were performed for each recognized particle. The AZtec software automatically applied a "ZAF" correction (PAP version of the f(pz) formalism (Pouchou and Pichoir, 1985) —considering atomic number (Z), absorption (A), and fluorescence (F)—to the raw data for elemental concentrations. Quantification was based on factory-delivered standard measurements. The ZAF correction assumes homogeneous samples with smooth surfaces perpendicular to the beam and thicknesses greater than the excitation volume—conditions not met by these particles due to their rough surfaces and small sizes. However, studies (Weinbruch et al., 1997; Meier et al., 2018; Kandler et al., 2018) have shown that for particles larger than 1 µm in diameter, the relative standard deviation of corrected concentrations of major elements is approximately 2%. For minor elements, the deviation is is higher. Since only particles with diameters > 1 µm in diameter were included in further data processing, the ZAF-corrected concentrations values were used without additional corrections. The standard deviation in ZAF-corrected concentrations measured in particles increases proportionally with the acceleration voltage (equivalent to increasing excitation volume). Several blank analyses of empty substrates have shown that under the applied analytical conditions, the substrate surface contains, in an area of ca. 1 mm^2, a maximum of five particles on unexposed substrates. These particles are

Moved up [1]: <#>developed by the National Oceanic and At (NOAA) Air Resources Laboratory (ARL) (Draxler and Rolph, 2003).

Deleted: se

Deleted: The forward calculations started from a point within satellite images.

Deleted: ¶

Deleted: ¶

Deleted: 3

Deleted: separated from bulk samples using an Olympus SZX

Deleted: previously¶ coated with 12 mm Pelco tabs (Ted Pella, Redding, CA, USA) boron substrates. The latter were¶ used to improve the contrast of low-atomic-number particles, s sample (area depending on particle¶ load on the sample surface) was

Deleted: also known as

Deleted: Zeiss Gemini 300 Field Emission Gun (FEG)-SEM

Deleted: n

Deleted: 80

Deleted: window

Deleted: Particle Vision

Deleted: For this purpose, a Zeiss Gemini 300 Field Emission an Oxford¶ X-MAX EDS detector with an 80 mm^2 window, a high-efficie Electron (BSE) detector, and¶ the particle analysis software included in AZtecFeature (Oxfor (Fribourg, Switzerland) was¶ used.

Deleted: A

Deleted: (A),

Moved down [2]: The ZAF procedure is valid only for homog surfaces perpendicular to the beam¶ and considerably thicker than the excitation volume. Neither c our case. However, several¶ authors (Weinbruch et al., 1997; Meier et al., 2018; Kandler et particles larger than 1 µm in¶ The ZAF correction ¶ and considerably thicker than the excitation volume. Neither c

Deleted: was applied automatically by the AZtec softv ... [1]

Moved (insertion) [2]

Deleted: diameteThe ZAF procedure is valid only for ... [2]

Deleted: ¶

Deleted: In contrast,

Deleted: considerably larger (Kandler et al., 2018)

Deleted: retained

Deleted: ¶

https://doi.org/10.5194/ar-2026-6
Preprint. Discussion started: 4 February 2026

organic in nature and most likely follicles.

2.5 Particle size and microstructure analysis

Images obtained from both the optical microscope and the SEM were used to characterize the particle-size distribution of the total dust and iberulites, as well as their microstructure, using Avizo software (Thermo Fisher). The selected iberulites were placed in a 1-inch round container and filled with impregnation resin. The resulting cylindrical samples were polished on the top side containing the iberulites and examined by electron microscopy. A BSE image of the polished section of an iberulite was also segmented using Avizo software (Thermo Fisher), enabling the counting of individual particles and the determination of their equivalent spherical diameter d_{ve}, defined as the diameter of a sphere with the same volume as the particle:

$$d_{ve} = \frac{1}{P^2}\sqrt{64\pi B^3} \quad (2)$$

with B representing the area covered by the particle on the sample substrate, and P the perimeter of the particle. Due to the resolution of the segmentation process, only particles larger than 0.05 µm can be recognized and counted. To compare the SMPS with the SEM-derived PSDs, the mobility diameter d_m obtained by SMPS must first be converted to the volume equivalent diameter d_{ve} (Decarlo et al., 2004):

$$d_{ve} = \frac{C_c(d_{ve})}{C_c(d_m)\chi} d_m = CF d_m \quad (3)$$

with $C_c(d_m)/C_c(d_{ve})$, the Cunningham slip correction factor ratio between the mobility and volume equivalent diameters, CF the conversion factor, and the dynamic shape factor χ:

$$\chi = \frac{F_P}{F_{ve}} \quad (4)$$

which is defined as the ratio of the drag force on the nonspherical particle F_P to the drag force on its volume equivalent sphere F_{ve} when both m[illegible]inds, 19 ($\chi = 1$) with the same velocity as the measured particle:

$$v_e = \frac{neC_c(d_m)}{3\pi\eta d_m} = \frac{neC_c(d_{ve})}{3\pi\eta\chi d_{ve}} \quad (5)$$

From equation (5), the conversion equation (3) follows. $C_c(d_{ve})$ is unknown. The ratio $C_c(d_m)/C_c(d_{ve})$ has, to our knowledge, been measured only for salt particles smaller than 600 nm. The latter (extrapolated for particles > 600 nm) was used to convert the volume-equivalent diameter into the mobility diameter. It is always less than one, increases with size, and decreases with aspect ratio. The axis ratios b/a (AR, the ratio of the longest dimension b to the orthogonal width a) and shape factors appear to depend on size, flow regime (Alexander et al., 2016), and orientation (Cheng et al., 1988) , ranging from near unity for smaller particles to a value of 3 for the largest particles. The average inside the iberulites is 1.46, close to 1.4 reported for dust particles in the 2 to 10 µm range. Overall, CF is mostly smaller than 1.0. The converted volume-equivalent diameters are smaller than the mobility diameters.

Deleted: The measurement voltage (12 kV)

Deleted: particle size distribution of the total dust, iberulites,

Deleted: with a FEI Sirion FEG microscope (20 kV) equipped detector with an 80 mm² window, a high-efficiency four-quad AZtecFeature software (Oxford Instruments) the same EDS sy mentioned earlier.

Deleted: .¶

Deleted: ¶

Commented [JR3]: Are you sure this number is correct? 50 nm?
Just to be sure

Deleted: (Decarlo

Deleted:

Deleted: et al., 2004):¶

Deleted: ¶

Deleted: □

Deleted: F_{ve}, when

Deleted: C_c

Deleted: C_c

Deleted: , and overall, CF is mostly smaller than the correspo

Deleted: <#>is the lowest possible to excite characteristic X-r in the sample. Several blank analyses of empty¶

https://doi.org/10.5194/ar-2026-6
Preprint. Discussion started: 4 February 2026

2.4 X-ray diffraction

A loose single dust particle sample, containing no iberulites but collected during the same period when the iberulites fell in Fribourg, was analyzed with a Rigaku Ultima IV diffractometer equipped with a Position Sensitive Detector (PSD). Diffractograms were recorded from 5° to 70° 2θ in step-scan mode (0.02°/step and 1 min/°). The copper X-ray tube was operated at 40 kV and 40 mA. The CuKa-radiation was filtered with a nickel foil. Quantitative phase analysis by Rietveld refinement (Bish and Post, 1993) was performed on the recorded patterns using the PDXL2 software package (Rigaku). The refined instrumental parameters are the zero shift, the sample displacement, and the peak shape, modelled using a Pseudo-Voigt profile. The structure parameters for the phases present in the sample were taken from the International Centre for Diffraction Data database, but only the scale factor, the unit-cell parameters, the isotropic overall temperature factor, and, in some cases, the preferred-orientation parameter (phyllosilicates, calcite) were refined using the March-Dollase (Dollase, 1986)formalism. The fractions of the phases present were determined through the scale factors. The atomic positions and site occupancies were held fixed during refinement. Iterations were performed until the refinement converged.

3 Results

3.1 Dust source and trajectory

For air masses arriving at 2000, 2500, and 3000 m ASL over Fribourg in the early afternoon of February 6th, HYSPLIT back-trajectory calculations were performed for hourly arrival times from 9:00 to 15:00 h.

Deleted: <#>boron substrates have shown that under the appli
substrate surface contains only the element boron¶
and that in an area of ca. 1 mm², a maximum of five particles
substrates. These particles are organic¶
in nature and most likely follicles. Images obtained with both
SEM were used to characterize¶
the size distribution of the iberulites and their microstructure u
Fisher).¶
The picked iberulites were placed in a round 1-inch container
resin. The resulting cylindrical¶
samples were polished on the top side containing the iberulites
FEG microscope (20 kV)¶
equipped with the same EDS system as the Zeiss microscope
polished section was also segmented¶
using Avizo software (Thermo Fisher), allowing the counting
determination of their equivalent¶
spherical diameter, as well as the corresponding size distributi
segmentation process, only¶
particles larger than 0.05 µm are possible to be recognized and
¶

Deleted: ¶

Deleted: .

https://doi.org/10.5194/ar-2026-6
Preprint. Discussion started: 4 February 2026

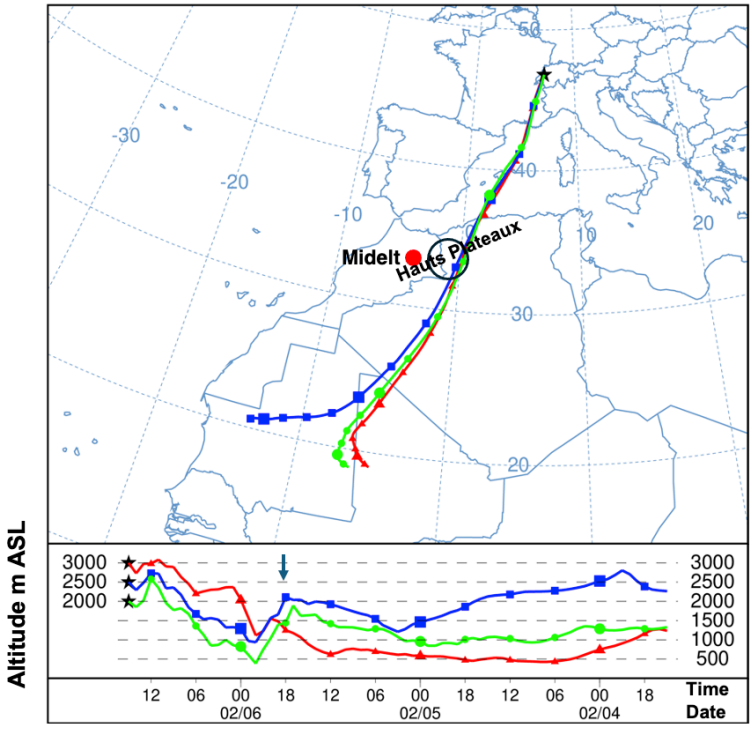

Figure 2: Back trajectories for air masses arriving over Payerne at 15:00 UTC, February 6th. The black circle shows the location of the first appearance of the dust plume entrained across the Mediterranean Sea towards central Europe. The black arrow points to the location markers inside the black circle.

The dust originated in northwest Africa (Fig. 2), between the southern Moroccan border and northwestern Algeria. Satellite images showed a dust plume forming in a region called "Hauts Plateaux" (also known as "Hautes Plaines") between the Pre-Sahara and the Tell Atlas (Fig.3). The air masses arriving over the Hauts Plateaux during the early afternoon of February 5th were at altitudes ranging between 1500 m to 3500 m AGL, which is within the Planetary Boundary Layer (PBL; calculated with the READY software (Rolph et al., 2017)), spanning from 2600 to 4500 m.

Deleted: Fig. 2.
Deleted: (see supplement 1)
Deleted: <#>The HYSPLIT backtrajectory calculations for air the early afternoon of February 6th¶ originated in NW Africa
Deleted: (Fig. 1) between the southern Moroccan border and r Satellite images¶ showed the appearance of a dust plume (Fig. 2)
Deleted: and evening
Deleted: over the Haut Plateau a
Deleted: 1000 m and 2000 m
Deleted: i.e., well
Deleted: (Fig. 4).
Deleted: (PBL, Fig. 3).
Deleted: On February 5th, the upper limit of the PBL in the H

https://doi.org/10.5194/ar-2026-6
Preprint. Discussion started: 4 February 2026

Surface wind velocity (10 m above ground) increased from 40 km/h to about 70 km/h.

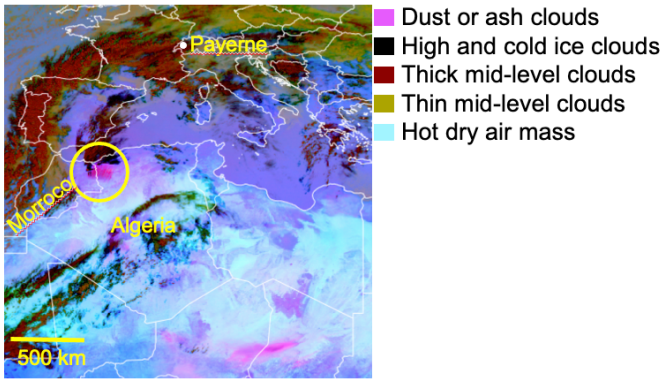

Figure 3: Satellite RGB image (5.2.2021. 22:00 UTC) from the SEVIRI dust product. The dust plume transported to Central Europe is seen east of the

Weather stations in the Atlas Mountains recorded hurricane-force gusts (e.g., 117 km/h on 05.02.21 in Midelt, Morocco (Hoshyaripour, 2021). This is clearly above the threshold wind speed for dust emissions given for western Algeria (Marticorena et al., 1997). The dust plume was transported northeastward toward the Mediterranean Sea, where a low-pressure system formed. The associated warm conveyor belt lifted the dust to higher altitudes and transported it with the polar jet across the Mediterranean toward the Alps, a process known as an "atmospheric river" (Francis et al., 2022; Rautela et al., 2024). Source sensitivities (the probability that an air mass originates from a given source along a certain path) for Saharan dust (fine mode) arriving at JFJ were calculated using FLEXPART to generate backward trajectories and assess the general surface contact of air masses over the Sahara Desert (Collaud Coen et al., 2025). The sensitivities indicate that the most common pathway is from the Sahara, over the Mediterranean, directly to the Alps.

3.2 Local meteorology

Ground temperature measurements and the T/RH profiles from the radio sonde released at 11:00 UTC in Payerne revealed relatively high temperatures for February 6th in Western Switzerland (4° C at the ground and a 0°C level at 2500 m ASL) and along with a typical inversion situation (Fig. 4). Compared to conditions during previous IFs over the Iberian Peninsula (Diaz-Hernandez and Sanchez-Navas, 2016) the temperature was much lower. The vertical profile of

Deleted: 3500 m AGL, and the velocity in the surface air laye
Deleted: ¶
Deleted: ¶
Deleted: ¶
152¶
<object>Figure 1: Back trajectories for air masses arriving ov
2000m AGL during February 6th between 12:00 and 18:00 UT
location of the first appearance of the dust plume entrained acr
towards central Europe .¶
Section Break (Next Page)
152¶
<object>Figure 1: Back trajectories for air masses arriving ov
2000m AGL during February 6th between 12:00 and 18:00 UT
location of the first appearance of the dust plume entrained acr
towards central Europe .¶
Section Break (Next Page)
<object>Figure 1: Back trajectories for air masses arriving ov
2000m AGL during February 6th between 12:00 and 18:00 UT
location of the first appearance of the dust plume entrained acr
towards central Europe .¶
Section Break (Next Page)
¶
¶
¶
<object>Figure 2: Satellite RGB image (5.2.2021. 22:00 UT
SEVIRI dust product, showing the presence of dust by pink co
to Central Europe is seen east of the Moroccan – Algerian bor
¶
¶
¶
¶
¶
¶
¶
¶
¶
¶
¶
¶
¶
¶
¶
¶
¶
¶
¶
¶
¶
... [3]
Deleted: entrained in a NE direction
Deleted: ¶
Deleted: ¶
Sea toward the Alps, a process referred to as an "atmospheric r
Rautela et al., 2024). Source¶
sensitivities were calculated for Saharan dust (fine mode) arriv
obtain the backward trajectories¶
Deleted: ¶
Deleted:
Deleted: ¶

https://doi.org/10.5194/ar-2026-6
Preprint. Discussion started: 4 February 2026

relative humidity (RH) was complex. RH decreased from 97% at the ground level to a very low 48 % at 1000 m, then increased to 61% at 3500 m ASL (Fig. 4). RH remained between 48 and 55% up to an altitude of 4300 m ASL, where it began to increase to 97 % resulting in a 100 m thick layer between 5000 and 5100 m ASL with temperatures below the frost point.

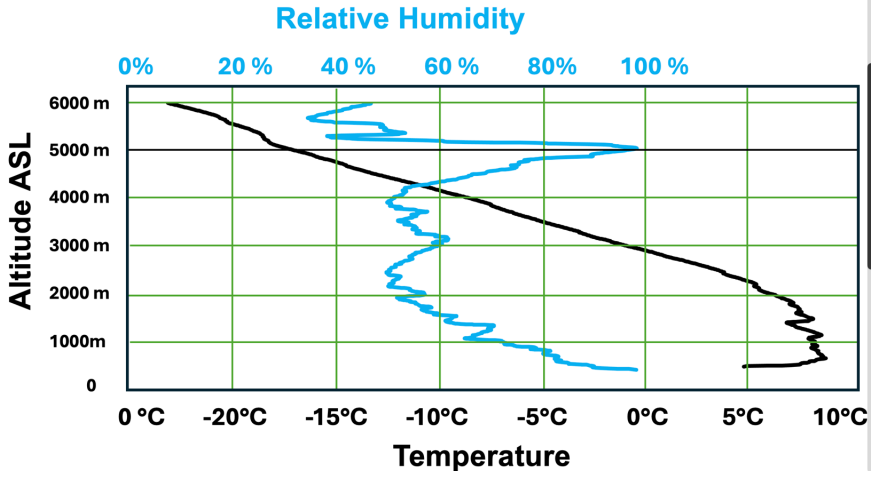

Figure 4: Temperature (black line) and relative humidity (blue line) as a function of altitude from the radio sounding. The balloon was released in Payerne at 11:00 h UTC. The balloon flew 30 km to the NW during the above recording (MeteoSwiss).

The Payerne ceilometer time profile (Fig. 5) shows a cloud base at 5000 m ASL at midnight, with reflections that may be due to aerosol (SDE) or ice particles, extending from the cloud base down to 3500 m. Early in the morning, the cloud base lowered to 4000 m, and the reflections extended down to 2500 m. The below-cloud reflections have a streaky appearance in the ceilogram. After a large gap in ceilometer recordings between 9:00 and 11:00 h UTC, a reflection wall extending from 3500m to the ground appeared. These strong reflections from dust particles persisted throughout the day. The cloud base lowered from 4000 m to 2000 m during the evening. At around 22:30 h, three short periods with very strong reflections were observed; during those times, precipitation was recorded on the ground. After 23:00 h, the reflections became less intense.

Deleted:
Deleted: ¶
Deleted:
Deleted: Fig. 3. T
Deleted: The balloon
Deleted:
Deleted:
Deleted:
Deleted:
Deleted:
Deleted:
Deleted: ¶

https://doi.org/10.5194/ar-2026-6
Preprint. Discussion started: 4 February 2026

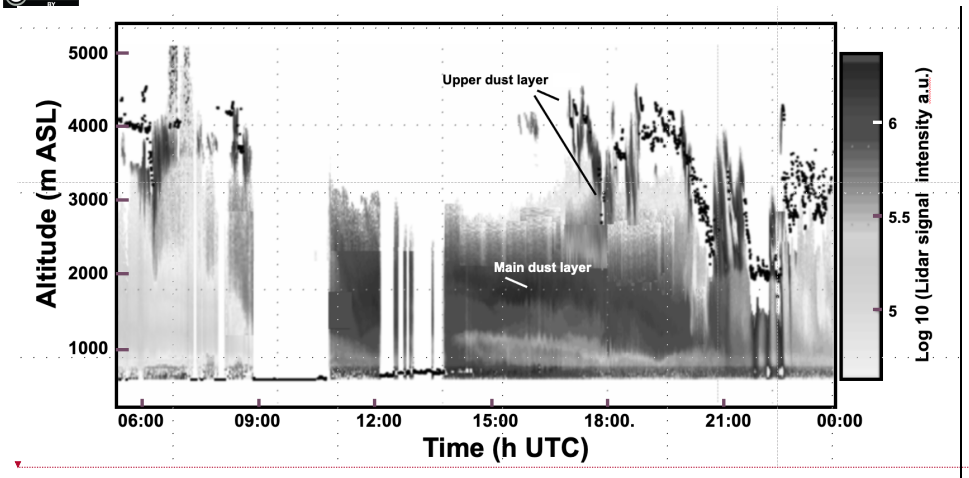

Figure 5: Ceilogram Ceilometer profile for February 6th (MeteoSwiss). The little black dots on top of the reflections show the meteorological clouds' bottom. The white stripes are gaps due to ground fog.

Lidar measurements were taken between 15:00 and 17:00, during the signal's peak values and the average was used to derive a mass-concentration profile (Fig. 6) across the dust cloud. The altitude range of 4000-5000 meters served as the "no aerosol" reference. The profile was derived using a lidar ratio of 0.57 $m^2/sr \pm$ sr at 532 nm (Haarig et al., 2022), an Ångström coefficient of 0.5 for long-range transported dust in northern European regions (Ansmann et al., 2001), and a mass extinction ratio at 532 nm of 0.47 ± 0.04 m^2 g^{-1} (Nemuc et al., 2013). The profile shows three peaks. The maximum concentration of 81 µg m^{-3} was observed at an altitude of 1675 m. The second-largest concentrationwas recorded just above the ground, and a third small peak was located just above the cloud base at approximately 3500m.

Deleted: <#>¶ ... [4]
Deleted: 181
Deleted: 5g. 4
Deleted: .
Deleted: e
Deleted: show themeteorological ¶
Deleted: 182
Deleted: ¶
Deleted: <#>¶
Deleted: 9¶
Deleted: ¶

https://doi.org/10.5194/ar-2026-6
Preprint. Discussion started: 4 February 2026

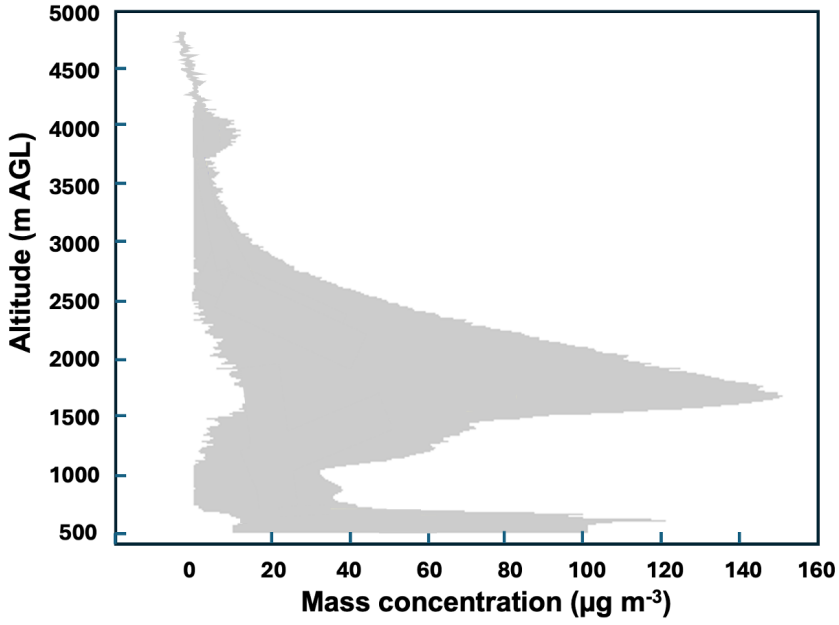

Figure 6: Aerosol mass concentration profile across the dust cloud calculated from the average of Lidar measurements taken between15:00 and 16:59 h (MeteoSwiss).

3.3 Morphology and microstructure of iberulites

Giant particles were previously observed following long-range transport of Saharan dust (Van Der Does et al., 2018). Rapid transport, high turbulence, and electrical forces are thought to counteract for the particles' weight. In our case, the large "particles" were not single particles but multimineral particle aggregates with spherical to slightly ellipsoidal shapes, known as iberulites after their first recording on the Iberian Peninsula (Fig. 7) (Díaz-Hernández and Párraga, 2008). The cores of the iberulites are composed mainly of coarser mineral grains (Fig. 8 e,f, and Fig. 9) that have accreted without a visible cement matrix. Except for a thin, dense surface layer, the iberulite cores show no internal structure, such as layering or preferential grain orientation. The iberulites collected in St Légier (n = 425) are larger than the Iberian specimens, with a mean diameter of 113 µm (range: 43 – 365 µm).

Deleted: Aerosol mass concentration profile across the dus

Deleted: <#>3.3 Iberulites collected in Fribourg and St. Lé
In Fribourg, very large particles with diameters exceeding 30 µ

Deleted: <#>single

Deleted: <#>have been

Deleted: <#>¶

Deleted: <#>previously

Deleted: gh¶

Deleted: compensate

Deleted: ¶

Deleted: ¶

Deleted: ¶

Deleted: ¶

Deleted: ¶

Deleted: ¶

https://doi.org/10.5194/ar-2026-6
Preprint. Discussion started: 4 February 2026

Figure 7: Light microscopy image of iberulites collected in St Légier.

Most iberulites have smooth surfaces with few large surface pores (Fig. 8 a-d), most likely due to particles ejected from the aggregates. Spherical surface depressions, e.g., vortices formed by airflow around aggregates, as observed on Iberian iberulites (Díaz-Hernand rulites.

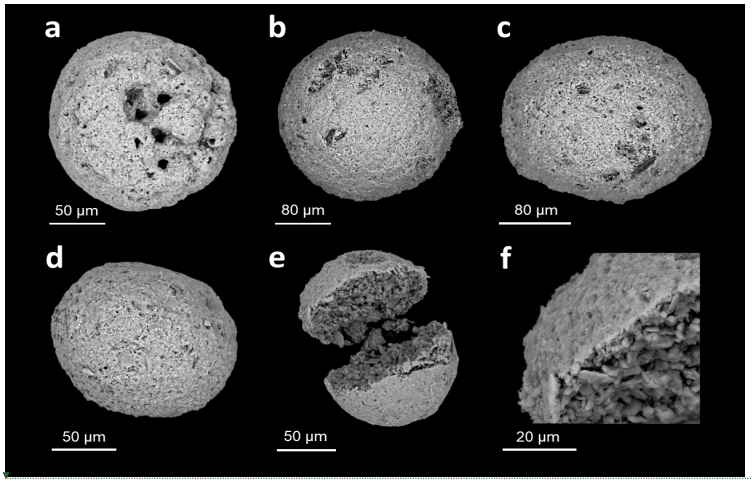

Figure 8: SEM images of some iberulites collected in St Légier on February 6th, 2021. Figure 8 f shows the fine-grained rim and the coarse-grained of an iberulite.

Moved (insertion) [4]
Deleted: .6
Deleted: .
Deleted: 7
Deleted: ejectedfrom
Moved (insertion) [5]
Deleted: ¶

https://doi.org/10.5194/ar-2026-6
Preprint. Discussion started: 4 February 2026

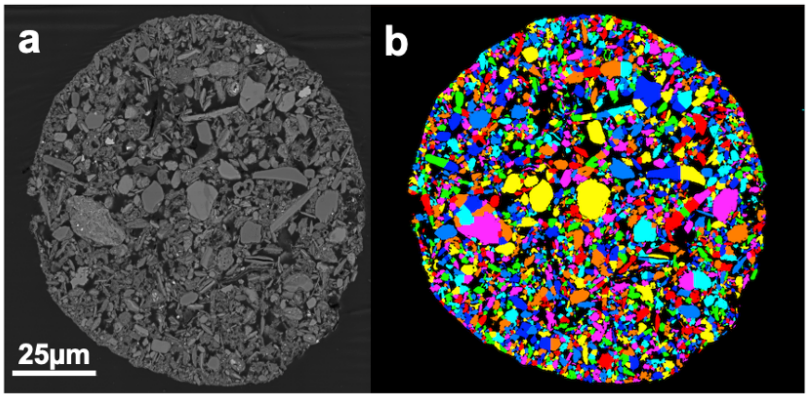

Figure 9: (a) BSE image of a polished section through an iberulite, and (b) the corresponding segmentation obtained from AVIZO. The different colors are used to better distinguish individual particles but do not represent any specific elemental composition.

Most iberulites have smooth surfaces with few large surface pores (Fig. 8), most likely due to particles that have been ejected from the aggregates. Spherical surface depressions, e.g., vortices formed by the flow of air around the aggregates, as observed on Iberian iberulites (Díaz-Hernández and Párraga, 2008), are very rare among the sampled iberulites.

3.4 PSDs at JFJ and inside the iberulites

During periods when JFJ is cloud-free, above the PBL, and free of Saharan dust, the PSD has two modes: a stronger one near 0.05 µm and a weaker one between 0.15 and 0.4 µm (Nessler et al., 2003; Bukowiecki et al., 2016, Cozic et al., 2008)(Fig. 10, green bars). The PSD measured at 11:00 UTC on February 6th during the SDE is monomodal, with maximum near 0.150 µm (see Fig. 10, yellow bars), and shows much higher concentrations than measurements without SDEs, similar to PSDs observed in previous Saharan dust episodes at JFJ (Chou et al., 2011). Coarse-mode particles arriving at JFJ were well documented in previous particle volume distributions, with a mode at 1.4 µm (Schwikowski et al., 1995). Saharan dust clouds transported over long distances, such as to Barbados during the SALTRACE campaign (Weinzierl et al., 2017), to Aeronet sites in the eastern Caribbean (Velasco-Merino et al., 2018), over the Mediterranean Sea during the ChArMEx/ADRIMED campaign (Denjean et al., 2016), and over Cape Verde during the SAMUN2 campaign (Weinzierl al., 2011) have similar PSDs. The largest particles observed at the Caribbean sites are well above the maximum diameter expected for settling due to Stokes' law during transport. The modes observed at JFJ and in the campaigns cited above are similar to the PSDs observed in the source regions (Panta et al., 2023; Bencherif et

Deleted: <#>Figure 8: SEM images of some iberulites collec 6th, 2021. Figure 8 f shows the fine-grained rim of an iberulite.

Deleted:

Deleted: v

Deleted: The long-term PSD measured with SMPS and CP cloud, was taken as representative of the

Deleted: PSD in the main dust layer. During times when JFJ i no Saharan dust present the

Deleted: s

Deleted: Herrmann et al., 2015;

Deleted:)

Deleted: (

Deleted: (Cozic et al., 2008)

Deleted: .

Deleted: a

Deleted:

Deleted:

Deleted:

Deleted:

Deleted:

Deleted: et

Deleted:

https://doi.org/10.5194/ar-2026-6
Preprint. Discussion started: 4 February 2026

al., 2022; Dubovik et al., 2006), but arelower in concentration and lack particles > 30µm.

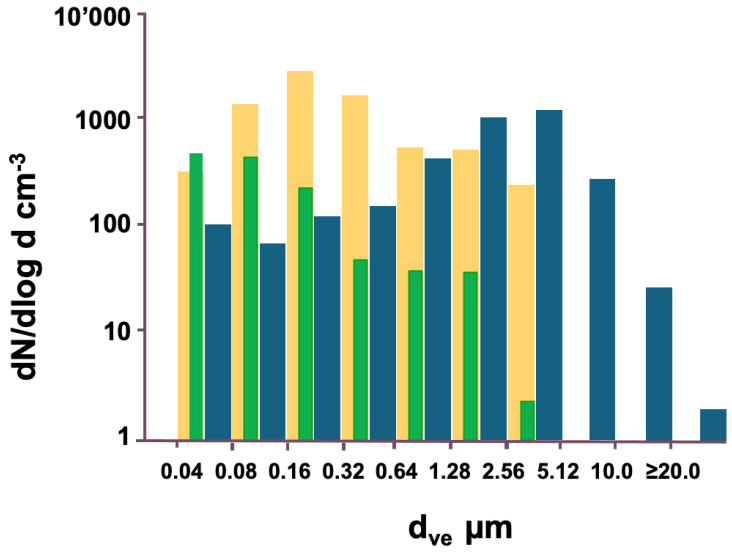

Figure 10: Jungfraujoch PSD measured in April 2004 during a period when JFJ was above the PBL, cloudfree and no SDE (green bars), during the SDE of February 6th at 12:00 (yellow bars, shifted 1bin to the left relative to the original data, s. text), and for an iberulite sample collected in St. Légier (blue bars).

Deleted: ¶

3.5 XRD -results (Rietveld analysis) and and EDS - analyses

X-ray diffraction showed that the dust contained phyllosilicates (illite, muscovite, and kaolinite, totaling 34.1 wt%), followed by carbonates (27.0 wt% calcite, 4.0 wt% dolomite) and quartz (23.3 wt%). The concentrations of gypsum and halite were below the detection limit. Analysis of individual particles within an iberulite confirms the XRD results. EDS analyses on the polished iberulite section have a resolution of 1–2 µm, depending on section thickness and local composition. Compositions of particles <1 µm should therefore be interpreted with caution. Trends from the ideal muscovite composition toward the calcite composition, as well as toward the quartz compositions, in the (Mg+Fe+Si+K–Al–Ca) ternary diagram indicate that the particles are mixtures of the three phases (Fig. 11 a). The ternary diagram (Mg+Fe+Si+K–S–Ca), with Mg+Fe+Si+K as the "silicate" corner and Ca as the "calcite" corner (Fig. 11 b), shows measurements mainly along the joint

Deleted: n.

https://doi.org/10.5194/ar-2026-6
Preprint. Discussion started: 4 February 2026

between the silicate and calcite corners, indicating mixed particles between these minerals, with some measurements scattered in the triangle silicates-calcite-gypsum, indicating mixed particles among these phases or the presence of sulfur on other particle surfaces.

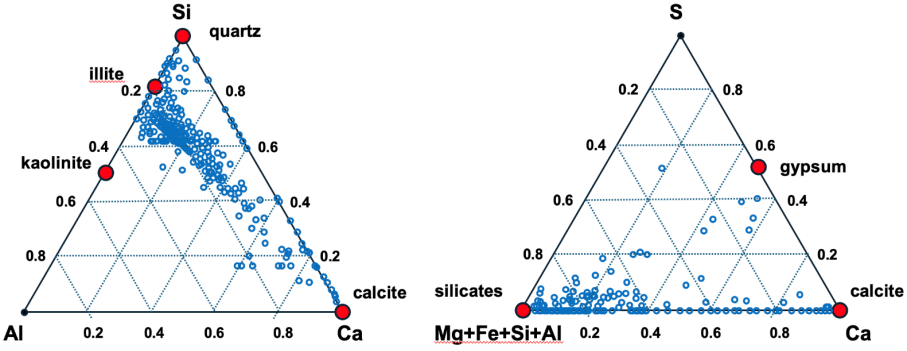

Figure 11: Ternary diagrams : (a) (Mg+Fe+Si+K–Al–Ca), (b) (Mg+Fe+Si+K–S–Ca).

4. Discussion

4.1 Dust compositio

Dust from potential source areas (PSA) has been characterized by bulk chemistry (Kandler et al., 2007) and mineralogy (Scheuvens et al., 2013). Mineralogical fingerprints include phyllosilicates, such as the ratio of illite to kaolinite concentrations (I/K) (Caquineau et al., 1998; Chester and Johnson, 1971; Scheuvens et al., 2013). In Northern Africa, the general trends are increases in I/K from S to N and from E to W. The value for the present samples is approximately 2.9, consistent with values reported from the Western Sahara, e.g., >2 in NW Algeria and Morocco. High carbonate contents (>10 wt.%, calcite > dolomite) are also a fingerprint of dust from the northwestern part of Africa (Avila et al., 1997). Similar to illite, carbonate content decreases continuously toward the south (Paquet, 1984). The high carbonate content of dust emitted from the northern regions within and adjacent to the Atlas Mountains reflects the geology of those regions (Grousset et al., 1992).

4.2 Iberulite formation and insights from internal structure

The layer at 5000 m altitude with supersaturated atmospheric conditions is most likely the source of the ice/snowflake

Deleted: 12
Moved (insertion) [9]
Deleted: n¶
Deleted: <#>¶
Deleted: ¶
Deleted: T
Deleted: ¶
Deleted: ¶
Deleted: ¶
Deleted: ¶
Deleted: ¶
Deleted: n¶
Moved up [3]: The Payerne ceilometer time profile (Fig. 5 ASL at midnight, with reflections that may be due¶
Moved (insertion) [8]
Deleted: 300¶
¶
X-ray diffraction (Fig. 11) showed that iberulites contain and kaolinite, totaling 34.1 wt%),¶
followed by carbonates (27.0 wt% calcite, 4.0 wt% dolom concentrations of gypsum and halite¶
were below the detection limit.¶
274¶
(MeteoSwiss)three peaks. The maximum concentration of altitude of 1675 m. The second-largest concentration¶
was recorded just above the ground, and a third small pe cloud base at approximately 3500 m.¶
¶
¶
typical inversion situation (Fig. 4a). In contrast to conditi the Iberian Peninsula (Diaz-Hernandez¶
and Sanchez-Navas, 2016) the temperature was much low relative humidity (RH) was complex. RH¶
<*object*>decreased from 100 % at the ground level to a ve increased to 85 % at 3500 m ASL (Fig. 4b).¶
¶
¶
¶
¶
¶
¶
¶
¶
¶
¶
The Payerne ceilometer time profile (Fig. 5) shows a clou midnight, with reflections that may be due¶
¶
169¶
Figure 4: Temperature (a) and relative humidity (b) as a radio sounding. The sounding balloon was release... [5]
Deleted: ¶

https://doi.org/10.5194/ar-2026-6
Preprint. Discussion started: 4 February 2026

precipitation that led to the formation of iberulites. The temperature at the upper boundary of the dust layer was below 0° C and turned positive around 2500 m. However, melting of the frozen hydrometeors most likely began at a much lower level due to the low relative humidity, in which the water vapor density of the surrounding air is lower than the equilibrium water vapor density of frozen hydrometeors at the freezing point; therefore, sublimation of water vapor occurs from the surface of the latter. Because of this sublimation process, latent cooling can push the surface temperature of the hydrometeor below 0 °C (Matsuo and Sasyo, 1981; Heymsfield et al., 2015). The width of the non-melting layer in the atmosphere increases nearly linearly with decreasing relative humidity, from 120 m at 90% to 700 m at 50%. The relative humidity at the top level of the main Sahara dust layer is around 70% and decreases with decreasing altitude. It is therefore probable that the melting level is displaced far into the massive Saharan dust layer. The layer at 5000 m altitude with supersaturated atmospheric conditions is most likely the source of the ice/snowflake precipitation that led to the formation of iberulites. Although difficult to distinguish from aerosol particles, the reflections just below the cloud base may originate from frozen hydrometeors. Both solid ice crystals and liquid drops can capture particles.

Several studies on BSC (Feng, 2009; Kyrö et al., 2009; Paramonov et al., 2011) indicate that frozen hydrometeors are more effective scavengers of aerosol particles than rain on an equivalent water-content basis. The fluttering, zigzagging fall style of frozen hydrometeors (Hashino et al., 2016; Kajikawa, 1992; Tagliavini et al., 2021; Mccorquodale and Westbrook, 2021; Stringham et al., 1969), prolongs their trajectories, thereby increasing the probability of collisions with aerosol particles and consequently, CE. CE also increases with temperature and relative humidity, although there is a discrepancy between experimental/natural data and theory (Santachiara et al., 2023). The highest CE has been recorded for mixed precipitation types and frozen hydrometeors at temperatures slightly above 0 °C. At these temperatures, frozen hydrometeors develop a stickier liquid layer at the surface. The increase in CE at higher RH is attributable to increased collector capacitance. (Paramonov et al., 2011). (Miller and Wang, 1989). The temperatures between the likely origin of the frozen hydrometeors and 2000 m ASL are in this range. The Greenfield gap for frozen hydrometeors fall situations was smaller, spanning 0.09-0.3 µm, compared to the gap observed for rain. This range is also observed for the iberulites collected in the present fieldwork, supporting frozen hydrometeors as dust scavengers. The increased CE of frozen hydrometeors is probably also the reason for the larger diameters observed in Swiss iberulites compared to Iberian iberulites. All frozen hydrometeors form thin liquid films on the surface and become stickier (Fujiyoshi, 1986; Knight, 1979; Leinonen and Lerber, 2018; Oraltay and Hallett, 2005). Large frozen hydrometeors increase in size through coalescence in the melting layer (Mcfarquhar et al., 2007). The behavior of scavenged aerosol particles within melting hydrometeors has not been analyzed to date. Most likely, they are incorporated into the newly formed raindrops. Within and below the melting layer, due to the very low relative humidity (45% at 1000 m, at the bottom of the massive dust layer), raindrops will dry very rapidly. A technological analog of this process is the (spray) drying of a powder suspension, which is used, e.g., in the ceramic, food, or pharmaceutical industry (Santos et al., 2018). The difference between the drying of a droplet in a spray drier and that of a rain droplet falling out of a cloud is the temperature difference between the droplet and the drying air stream, which is around 200°C in a spray drier. Droplets in a spray dryer relax into spherical shapes and are analogous to raindrops. The latent heat of water evaporation induces a strong heat flux from the droplet surface into the gas stream. This, in turn, drives thermophoretic particle displacement toward the droplet surface and a specific microcirculation in a layer near the surface, driven by the surface-tension gradient (Iskandar et al., 2003). This microcirculation entrains particles toward the droplet surface, leading to size- and density-based segregation. Smaller and/or less dense particles move faster toward the droplet surface, forming a surface layer. Coarser particles are concentrated in the core. Such a shell-core structure was observed in the present iberulite and has also been reported in the Iberian examples (Díaz-Hernández and Párraga, 2008; Párraga et al., 2021), with fine-grained phyllosilicates concentrated in the shell and coarse-grained quartz grains in the core. 5. Conclusion

5. Conclusions

To our knowledge, this analysis represents the first detailed study of iberulite fall in Switzerland. In contrast to the Iberian cases, the IF fall occurred under much colder conditions, e.g., temperatures around 0° and decreasing relative humidity along

Deleted: The IF on February 6th in Fribourg was observed in conditions during the fall are therefore well known. Two mechanisms have been proposed for aggregatin within a drop (Diaz-Hernandez and Sanchez-Navas, 2016; Párraga et al., 2021): 1. The coale increases the number of condensation nuclei within a single growing drop, i.e., in-clo denoted as 'nucleation scavenging'), or 2. the concentration increases through collisions between the cloud along its trajectory to the ground. This mechanism is called below-cloud scavenging (E scavenging) (Pruppacher and Klett, 2010). The BCS rate strongly depends on rainfall inten and the drop's ability to collect particles, called the collection efficiency (CE) (Volken and S Laakso et al., 2003). CE is the number (or mass) of particles captured by a drop of particle number in the cylindrical volume swept by the drop per unit trajectory length. If CE we of the drop, the particle, environmental parameters, and the capture processes, the gra would reflect the size distribution of the dust in the volume traversed by the drop. F Fig. 10). The mechanisms ... [6]

Deleted: ¶

Deleted: ¶

Deleted: ¶

Deleted: ¶

Deleted: ¶

Deleted: ¶

Deleted: ¶

Deleted: ¶

Deleted: ¶

Deleted: <#>Frozen hydrometeors can occur as small particles columnar or planar crystals (branched = snowflakes), ... [7]

Deleted: <#>e¶

Deleted: ¶

Deleted: ,

Deleted: ¶

Deleted: ¶

Deleted: ¶

Deleted: ¶

Moved up [10]: Within and below the melting layer, due to th (45% at 1000 m, at the bottom of the massive dust¶

Moved (insertion) [10]

Deleted: ¶ ¶ ... [8]

Deleted: ¶

Deleted: ¶

https://doi.org/10.5194/ar-2026-6
Preprint. Discussion started: 4 February 2026

the fall trajectory. Iberulites form through the accumulation of particles inside raindrops. A comparison of the PSD inside the iberulites with the PSD measured in the dust cloud at the Jungfraujoch, which encountered the same cloud, revealed a Greenfield gap in the iberulite PSD, i.e., a lack of particles in the range between 0.1 and 0.3 µm. The presence of a Greenfield gap within the iberulites supports below-cloud scavenging, i.e., particle capture through collisions of particles with droplets below a cloud, as the mechanism for particle accumulation. The gap arises from particle trajectories in the flow around the falling droplet, which depend on particle size. The freezing temperature, low relative humidity, and ceilogram signals suggest that particle collisions occurred not with raindrops but with snowflakes or ice crystals. The latter are known to be better scavengers than raindrops. Since 2021, more iberulites have been found in filter samples collected during SDEs in Switzerland. They will be analysed to confirm the findings and to gain a better understanding of the relationship between iberulite formation and meteorological conditions.

Author contributions

BG designed the study. CN, BG, and JR performed the measurements. BG analyzed the data. MS provided data from Jungfraujoch. BG, JI

Competing interests

The authors declare that they have no conflict of interest..

Acknowledgements

The authors acknowledge Maxime Hervo from Meteoswiss for the supply of meteorological and lidar data. We thank also Mario Wannier for supp
from JFJ.

~~**Financial support**~~

This research received no external funding.

Deleted: ¶
Deleted: ¶
Deleted: ¶
Deleted: ¶
Deleted: ¶
Deleted: ¶
Deleted: ¶
Deleted: ¶
Deleted: ¶
Deleted: ¶

Deleted: References¶
¶
Alexander, J. M., Bell, D. M., Imre, D., Kleiber, P. D., Grass
Measurement of size-dependent dynamic shape factors of qua
Aerosol Science and Technology, 50, 870–879, 10.1080/027
Ansmann, A., Bösenberg, J., Chaikovsky, A., Comerón, A., I
Freudenthaler, V., Ginoux, P., Komguem, L., Linnè, H., Linr
Matthias, V., Mattis, I., Mitev, V., Müller, D., Music, S., Nic
Sobolewsky, P., Srivastava, M. K., Stohl, A., Torres, O., Vau
Wiegner, M.: Longr range transport of Saharan dust to northe
2001 outbreak observed with EARLINET, Journal of Geophy
108, 4783, 10.1029/2003JD003757i, 2001.¶
Ashpole, I. and Washington, R.: A new high-resolution centr
summertime dust source map from automated satellite dust p
Geophysical Research Atmospheres, 118, 6981–6995, 10.100
Avila, A., Queralt-Mitjans, I., and Alarcón, M.: Mineralogica
delivered by red rains over northeastern Spain, Journal of Ge
102, 21977–21996, 10.1029/97jd00485, 1997.¶
Barthazy, E., Henrich, W., and Waldvogel, A.: Size distributi
melting layer, Atmospheric Research, 47-48, 193–208, 10.10
1998.¶
Bencherif, H., Bounhir, A., Bègue, N., Millet, T., Benkhaldo
and Gadouali, F.: Aerosol distributions and Sahara dust trans
ground-based and satellite observations, Remote Sensing, 14
Bish, D. L. and Post, J. E.: Quantitative mineralogical analys
fitting method, American Mineralogist, 78, 10.2138/am-1993
Bukowiecki, N., Weingartner, E., Gysel, M., Coen, M. C., Zi
Steinbacher, M., Ga¨ggeler, H. W., and Baltensperger, U.: A
aerosol observation at the high altituder research station Jung
asl), Aerosol and Air Quality Research, 16, 764–788, 10.420
Buseck, P. R. and Pósfai, M.: Airborne minerals and related a
climate and the environment, Proceedings of the National Ac
States of America, 96, 10.1073/pnas.96.7.3372, 1999.¶
Caquineau, S., Gaudichet, A., Gomes, L., Magonthier, M. C.
Clay ratio as a relevant tracer to assess the origin of soil-deriv
Research Letters, 25, 983–986, 10.1029/98GL00569, 1998.C
Allen, M. D.: Dynamic Shape Factor of a Plate-Like Particle,
Technology, 8, 109–123, 10.1080/02786828808959176, 198
Chester, R. and Johnson, L. R.: Atmospheric dusts collected
Africa and the Iberian Peninsula, Marine Geology, 11, 251–2
3227(71)90027-2, 1971.¶
... [9]

Deleted: 604¶
605¶
606¶
607¶
... [10]

References

Alexander, J. M., Bell, D. M., Imre, D., Kleiber, P. D., Grassian, V. H., and Zelenyuk, A.: Measurement of size-dependent dynamic shape factors of quartz particles in two flow regimes, Aerosol Science and Technology, 50, 870–879, 10.1080/02786826.2016.1200006, 2016.

Ansmann, A., Bösenberg, J., Chaikovsky, A., Comerón, A., Eckhardt, S., Eixmann, R., Freudenthaler, V., Ginoux, P., Komguem, L., Linnè, H., Linné, H., Márquez, M. A. N. L., Matthias, V., Mattis, I., Mitev, V., Müller, D., Music, S., Nickovic, S., Pelon, J., Sauvage, L., Sobolewsky, P., Srivastava, M. K., Stohl, A., Torres, O., Vaughan, G., Wandinger, U., and Wiegner, M.: Longr range transport of Saharan dust to northern Europe: The 11th October 2001 outbreak observed with EARLINET, Journal of Geophysical Research: Atmospheres, 108, 4783, 10.1029/2003JD003757ï, 2001.

Avila, A., Queralt-Mitjans, I., and Alarcón, M.: Mineralogical composition of African dust delivered by red rains over northeastern Spain, Journal of Geophysical Research Atmospheres, 102, 21977–21996, 10.1029/97jd00485, 1997.

Bencherif, H., Bounhir, A., Bègue, N., Millet, T., Benkhaldoun, Z., Lamy, K., Portafaix, T., and Gadouali, F.: Aerosol Distributions and Sahara Dust Transport in Southern Morocco, from Ground-Based and Satellite Observations, Remote Sensing, 14, 10.3390/rs14102454, 2022.

Bish, D. L. and Post, J. E.: Quantitative mineralogical analysis using the Rietveld full-pattern fitting method, American Mineralogist, 78, 1993.

Brem, B., Gysel, M., and Gysel-Beer, M.: EMEP, CREATE, ACTRIS, GAW-WDCA, 2020-2023, Particle number size distribution at Jungfraujoch, EBAS at NILU [dataset], 10.48597/MNVM-38BX, 2023.

Brennan, K. P. and Wilhelm, L.: Saharan dust linked to European hail events, Atmospheric Chemistry and Physics, 25, 10823–10836, 10.5194/acp-25-10823-2025, 2025.

Bukowiecki, N., Weingartner, E., Gysel, M., Coen, M. C., Zieger, P., Herrmann, E., Steinbacher, M., Ga¨ggeler, H. W., and Baltensperger, U.: A Review of More than 20 Years of Aerosol Observation at the High Altitude Research Station Jungfraujoch, Switzerland (3580 m asl), Aerosol and Air Quality Research, 16, 764–788, 10.4209/aaqr.2015.05.0305, 2016.

Buseck, P. R. and Pósfai, M.: Airborne minerals and related aerosol particles: Effects on climate and the environment, Proceedings of the National Academy of Sciences of the United States of America, 96, 10.1073/pnas.96.7.3372, 1999.

Caquineau, S., Gaudichet, A., Gomes, L., Magonthier, M. C., and Chatenet, B.: Saharan dust: Clay ratio as a relevant tracer to assess the origin of soil-derived aerosols, Geophysical Research Letters, 25, 983–986, 10.1029/98GL00569, 1998.

Cheng, Y.-S., Yeh, H.-C., and Allen, M. D.: Dynamic Shape Factor of a Plate-Like Particle, Aerosol Science and Technology, 8, 109–123, 10.1080/02786828808959176, 1988.

Chester, R. and Johnson, L. R.: Atmospheric dusts collected off the Atlantic coasts of North Africa and the Iberian Peninsula, Marine Geology, 11, 251–260, 10.1016/0025-3227(71)90027-2, 1971.

Chou, C., Stetzer, O., Weingartner, E., Jurányi, Z., Kanji, Z. A., and Lohmann, U.: Ice nuclei properties within a Saharan dust event at the Jungfraujoch in the Swiss Alps, Atmospheric Chemistry and Physics, 11, 4725–4738, 10.5194/acp-11-4725-2011, 2011.

Coen, M. C., Weingartner, E., Schaub, D., Hueglin, C., Corrigan, C., Henning, S., Schwikowski, M., and Baltensperger, U.: Saharan dust events at the Jungfraujoch: detection by wavelength dependence of the single scattering albedo and first climatology analysis, Atmospheric Chemistry and Physics, 4, 2465–2480, 10.5194/acp-4-2465-2004, 2004.

Collaud Coen, M., Brem, B. T., Gysel-Beer, M., Modini, R., Henne, S., Steinbacher, M., Putero, D., Gini, M. I., and Eleftheriadis, K., 10.5194/egusphere-2025-4162, 2025.

Cozic, J., Verheggen, B., Weingartner, E., Crosier, J., Bower, K. N., Flynn, M., Coe, H., Henning, S., Steinbacher, M., Henne, S., Collaud Coen, M., Petzold, A., and Baltensperger, U.: Chemical composition of free tropospheric aerosol for PM1 and coarse mode at the high alpine site Jungfraujoch, Atmospheric Chemistry and Physics, 8, 407–423, 10.5194/acp-8-407-2008, 2008.

Cuevas-Agulló, E., Barriopedro, D., García, R. D., Alonso-Pérez, S., González-Alemán, J. J., Werner, E., Suárez, D., Bustos, J. J., García-Castrillo, G., García, O., Barreto, Á., and Basart, S.: Sharp increase in Saharan dust intrusions over the western Euro-Mediterranean in February–March 2020–2022 and associated atmospheric circulation, Atmospheric Chemistry and Physics, 24, 4083–4104, 10.5194/acp-24-4083-2024, 2024.

Formatted: Justified, Indent: Left: 0"

Formatted: No bullets or numbering

Formatted: Left: 0.63", Section start: New page, Numbering: Continuous

DeCarlo, P. F., Slowik, J. G., Worsnop, D. R., Davidovits, P., and Jimenez, J. L.: Particle Morphology and Density Characterization by Combined Mobility and Aerodynamic Diameter Measurements. Part 1: Theory, Aerosol Science and Technology, 38, 1185–1205, 10.1080/027868290903907, 2004.

Denjean, C., Cassola, F., Mazzino, A., Triquet, S., Chevaillier, S., Grand, N., Bourrianne, T., Momboisse, G., Sellegri, K., Schwarzenbock, A., Freney, E., Mallet, M., and Formenti, P.: Size distribution and optical properties of mineral dust aerosols transported in the western Mediterranean, Atmospheric Chemistry and Physics, 16, 1081–1104, 10.5194/acp-16-1081-2016, 2016.

Diaz-Hernandez, J. L. and Sanchez-Navas, A.: Saharan dust outbreaks and iberulite episodes, Journal of Geophysical Research, 121, 10.1002/2016JD024913, 2016.

Díaz-Hernández, J. L. and Párraga, J.: The nature and tropospheric formation of iberulites: Pinkish mineral microspherulites, Geochimica et Cosmochimica Acta, 72, 3883–3906, 10.1016/j.gca.2008.05.037, 2008.

Dollase, W. A.: Correction of intensities for preferred orientation in powder diffractometry: application of the March model, Journal of Applied Crystallography, 19, 267–272, 10.1107/s0021889886089458, 1986.

Draxler, R. R. and Rolph, G. D.: HYSPLIT (HYbrid Single-Particle Lagrangian Integrated Trajectory), NOAA Air Resources Laboratory, College Park, MD, 2003.

Dubovik, O., Sinyuk, A., Lapyonok, T., Holben, B. N., Mishchenko, M., Yang, P., Eck, T. F., Volten, H., Muñoz, O., Veihelmann, B., van der Zande, W. J., Leon, J. F., Sorokin, M., and Slutsker, I.: Application of spheroid models to account for aerosol particle nonsphericity in remote sensing of desert dust, Journal of Geophysical Research: Atmospheres, 111, 10.1029/2005jd006619, 2006.

Feng, I. Y., Gill, T. E., Van Pelt, R. S., Webb, N. P., and Tong, D. Q.: Economic costs of wind erosion in the United States, Nature Sustainability, 8, 307–314, 10.1038/s41893-024-01506-4, 2025.

Feng, J.: A 3-mode parameterization of below-cloud scavenging of aerosols for use in atmospheric dispersion models, Atmospheric Environment, 41, 6808–6822, 10.1016/j.atmosenv.2007.04.046, 2007.

Fischer, A. and Hüglin, C.: Partikelmessungen im NABEL, Messbericht 2024, Empa, Abteilung Luftfremdstoffe/Umwelttechnik, Dübendorf, 2024.

Flentje, H., Briel, B., Beck, C., Collaud Coen, M., Fricke, M., Cyrys, J., Gu, J., Pitz, M., and Thomas, W.: Identification and monitoring of Saharan dust: An inventory representative for south Germany since 1997, Atmospheric Environment, 109, 87–96, 10.1016/j.atmosenv.2015.02.023, 2015.

Francis, D., Eayrs, C., Chaboureau, J. P., Mote, T., and Holland, D. M.: Polar Jet Associated Circulation Triggered a Saharan Cyclone and Derived the Poleward Transport of the African Dust Generated by the Cyclone, Journal of Geophysical Research: Atmospheres, 123, 10.1029/2018jd029095, 2018.

Francis, D., Fonseca, R., Nelli, N., Bozkurt, D., Picard, G., and Guan, B.: Atmospheric rivers drive exceptional Saharan dust transport towards Europe, Atmospheric Research, 266, 10.1016/j.atmosres.2021.105959, 2022.

Fujiyoshi, Y.: Melting Snowflakes, Journal of the Atmospheric Sciences, 43, 307–311, 10.1175/1520-0469(1986)043<0307:MS>2.0.CO;2, 1986.

Fussell, J. C. and Kelly, F. J.: Mechanisms underlying the health effects of desert sand dust, Environment Intternational, 157, http://dx.doi.org/10.60910/4x9t-ghuu, 2021.

Grousset, F. E., Rognon, P., Coudé-Gaussen, G., and Pédemay, P.: Origins of peri-Saharan dust deposits traced by their Nd and Sr isotopic composition, Palaeogeography, Palaeoclimatology, Palaeoecology, 93, 203–212, 10.1016/0031-0182(92)90097-O, 1992.

Haarig, M., Ansmann, A., Engelmann, R., Baars, H., Toledano, C., Torres, B., Althausen, D., Radenz, M., and Wandinger, U.: First triple-wavelength lidar observations of depolarization and extinction-to-backscatter ratios of Saharan dust, Atmospheric Chemistry and Physics, 22, 355–369, 10.5194/acp-22-355-2022, 2022.

Hashino, T., Cheng, K. Y., Chueh, C. C., and Wang, P. K.: Numerical study of motion and stability of falling columnar crystals, Journal of the Atmospheric Sciences, 73, 1923–1942, 10.1175/JAS-D-15-0219.1, 2016.

Deleted: http://dx.doi.org/10.60910/4x9t-ghuu,

Heald, C. L., Ridley, D. A., Kroll, J. H., Barrett, S. R. H., Cady-Pereira, K. E., Alvarado, M. J., and Holmes, C. D.: Contrasting the direct radiative effect and direct radiative forcing of aerosols, Atmospheric Chemistry and Physics, 14, 5513–5527, 10.5194/acp-14-5513-2014, 2014.
Heymsfield, A. J., Bansemer, A., Poellot, M. R., and Wood, N.: Observations of ice microphysics through the melting layer, Journal of the Atmospheric Sciences, 72, 2902–2928, 10.1175/JAS-D-14-0363.1, 2015.
Hinds, W. C.: Aerosol Technology, John Wiley and Sons, New York1999.
Hüglin, C., Grange S.K.: Chemical characterisation and source identification of PM10 and PM2.5 in Switzerland, EMPA, Dübendorf, EMPA, Dübendorf, 2021.
Iskandar, F., Chang, H., and Okuyama, K.: Preparation of microencapsulated powders by an aerosol spray method and their optical properties, Advanced Powder Technology, 14, 349–367, 10.1163/15685520360685983, 2003.
Jones, N. R., de Jersey, A. M., Lavers, J. L., Rodemann, T., and Rivers-Auty, J.: Identifying laboratory sources of microplastic and nanoplastic contamination from the air, water, and consumables, J Hazard Mater, 465, 133276, 10.1016/j.jhazmat.2023.133276, 2024.
Jurányi, Z., Gysel, M., Weingartner, E., Bukowiecki, N., Kammermann, L., and Baltensperger, U.: A 17 month climatology of the cloud condensation nuclei number concentration at the high alpine site Jungfraujoch, Journal of Geophysical Research, 116, 10.1029/2010jd015199, 2011.
Kajikawa, M.: Observations of the Falling Motion of Plate-Like Snow Crystals Part I: The Free-Fall Patterns and Velocity, Journal of the Meteorological Society of Japan. Ser. II, 70, 1–9, 10.2151/jmsj1965.70.1_1, 1992.
Kandler, K., Schneiders, K., Ebert, M., Hartmann, M., Weinbruch, S., Prass, M., and Pöhlker, C.: Composition and mixing state of atmospheric aerosols determined by electron microscopy: Method development and application to aged Saharan dust deposition in the Caribbean boundary layer, Atmospheric Chemistry and Physics, 18, 13429–13455, 10.5194/acp-18-13429-2018, 2018.
Kandler, K., Benker, N., Bundke, U., Cuevas, E., Ebert, M., Knippertz, P., Rodríguez, S., Schütz, L., and Weinbruch, S.: Chemical composition and complex refractive index of Saharan Mineral Dust at Izaña, Tenerife (Spain) derived by electron microscopy, Atmospheric Environment, 41, 8058–8074, 10.1016/j.atmosenv.2007.06.047, 2007.
Kearsley, A. T., Burchell, M. J., Hörz, F., Cole, M. J., and Schwandt, C. S.: Laboratory simulation of impacts on aluminum foils of the Stardust spacecraft: Calibration of dust particle size from comet Wild-2, Meteoritics & Planetary Science, 41, 167–180, 10.1111/j.1945-5100.2006.tb00201.x, 2010.
Kellogg, C. A. and Griffin, D. W.: Aerobiology and the global transport of desert dust, Trends Ecol Evol, 21, 638–644, 10.1016/j.tree.2006.07.004, 2006.
Knight, C. A.: Observations of the morphology of melting snow, Journal of Atmospheric Sciences, 1123–1113o, 1979.
Kyrö, E.-M., Grönholm, T., Vuollekoski, H., Virkkula, A., Kulmala, M., Laakso, L., and Kyrö, E.: Snow scavenging of ultrafine particles: field measurements and parameterization, Boreal Environment Research, 14, 11, http://dx.doi.org/10.60910/4x9t-ghuu, 2009.
Leinonen, J. and Lerber, A. v.: Snowflake Melting Simulation Using Smoothed Particle Hydrodynamics, Journal of Geophysical Research: Atmospheres, 123, 1811–1825, 10.1002/2017JD027909, 2018.
Li, T., Cohen, A. J., Krzyzanowski, M., Zhang, C., Gumy, S., Mudu, P., Pant, P., Liu, Q., Kan, H., Tong, S., Chen, S., Kang, U., Basart, S., Toure, N. E., Al-Hemoud, A., Rudich, Y., Tobias, A., Querol, X., Khomsi, K., Samara, F., Hashizume, M., Stafoggia, M., Malkawi, M., Wang, S., Zhou, M., Shi, X., Jiang, G., and Shen, H.: Sand and dust storms: a growing global health threat calls for international health studies to support policy action, Lancet Planet Health, 9, e34–e40, 10.1016/S2542-5196(24)00308-5, 2025.
Lian, L., Huang, J., Chen, S., Du, S., Zhang, L., and Yang, J.: A Comprehensive Review of Dust Events: Characteristics, Climate Feedbacks, and Public Health Risks, Current Pollution Reports, 11, 10.1007/s40726-025-00347-9, 2025.
Marticorena, B., Bergametti, G., Aumont, B., Callot, Y., N'Doumé, C., and Legrand, M.: Modeling the atmospheric dust cycle 2. Simulation of Saharan dust sources, Journal of Geophysical Research Atmospheres, 102, 10.1029/96jd02964, 1997.
Matsuo, T. and Sasyo, Y.: Melting of Snowflakes below Freezing Level in the Atmosphere, Journal of the Meteorological Society of Japan. Ser. II, 59, 10–25, 10.2151/jmsj1965.59.1_10, 1981.

Deleted: February 2021: A dusty month for Europe: /blogs.egu.eu/divisions/as/2021/04/03/february-2021-a-dusty-month-for-europe/, last ¶

Deleted: http://dx.doi.org/10.60910/4x9t-ghuu

Matzenauer, E.: Tectonics of the Préalpes Klippen and the subalpine molasse (canton Fribourg, Switzerland) Geofocus, 31, doi.org/10.1080/17445647.2025.2509914, 2011.
Mauro, B. D., Garzonio, R., Rossini, M., Filippa, G., Pogliotti, P., Galvagno, M., Cella, U. M. D., Migliavacca, M., Baccolo, G., Clemenza, M., Delmonte, B., Maggi, V., Dumont, M., Tuzet, F., Lafaysse, M., Morin, S., Cremonese, E., and Colombo, R.: Saharan dust events in the European Alps: Role in snowmelt and geochemical characterization, Cryosphere, 13, 1147–1165, 10.5194/tc-13-1147-2019, 2019.
McCorquodale, M. W. and Westbrook, C. D.: TRAIL: A novel approach for studying the aerodynamics of ice particles, Quarterly Journal of the Royal Meteorological Society, 147, 589–604, 10.1002/qj.3935, 2021.
McFarquhar, G. M., Timlin, M. S., Rauber, R. M., Jewett, B. F., Grim, J. A., and Jorgensen, D. P.: Vertical Variability of Cloud Hydrometeors in the Stratiform Region of Mesoscale Convective Systems and Bow Echoes, Monthly Weather Review, 135, 3405–3428, 10.1175/MWR3444.1, 2007.
Meibodi, A. E., Abdoli, G., Taklif, A., and Morshedi, B.: Economic Modeling of the Regional Polices to Combat Dust Phenomenon by Using Game Theory, Procedia Economics and Finance, 24, 409–418, 10.1016/s2212-5671(15)00697-8, 2015.
Meier, M. F., Mildenberger, T., Locher, R., Rausch, J., Zünd, T., Neururer, C., Ruckstuhl, A., and Grobéty, B.: A model based two-stage classifier for airborne particles analyzed with Computer Controlled Scanning Electron Microscopy, Journal of Aerosol Science, 123, 1–16, 10.1016/j.jaerosci.2018.05.012, 2018.
Middleton, N. J.: Desert dust hazards: A global review, Aeolian Research, 24, 53–63, 10.1016/j.aeolia.2016.12.001, 2017.
Miller, N. L. and Wang, P. K.: Theoretical determination of the efficiency of aerosol particle collection by falling columnar ice crystals, J. ATMOS. SCI., 46, 1656–1663, 10.1175/1520-0469(1989)046<1656:TDOTEO>2.0.CO;2, 1989.
Nemuc, A., Vasilescu, J., Talianu, C., Belegante, L., and Nicolae, D.: Assessment of aerosol's mass concentrations from measured linear particle depolarization ratio (vertically resolved) and simulations, Atmospheric Measurement Techniques, 6, 3243–3255, 10.5194/amt-6-3243-2013, 2013.
Nessler, R., Bukowiecki, N., Henning, S., Weingartner, E., Calpini, B., and Baltensperger, U.: Simultaneous dry and ambient measurements of aerosol size distributions at the Jungfraujoch, Tellus B: Chemical and Physical Meteorology, 55, 10.3402/tellusb.v55i3.16371, 2003.
Oraltay, R. G. and Hallett, J.: The Melting Layer: A Laboratory Investigation of Ice Particle Melt and Evaporation near 0°C, Journal of Applied Meteorology and Climatology, 44, 206–220, 10.1175/jam2194.1, 2005.
Panta, A., Kandler, K., Alastuey, A., González-Flórez, C., González-Romero, A., Klose, M., Querol, X., Reche, C., Yus-Díez, J., and Pérez García-Pando, C.: Insights into the single-particle composition, size, mixing state, and aspect ratio of freshly emitted mineral dust from field measurements in the Moroccan Sahara using electron microscopy, Atmospheric Chemistry and Physics, 23, 3861–3885, 10.5194/acp-23-3861-2023, 2023.
Paquet, G., Rognon, P.,Coude-Gaussen G,,, Wendling R.: Etude minralogique de poussires sahariennes le long d'un itinraire entre 19 °et 35 °de latitude nord, Revue de géologie dynamique et de géographie physique, 25, 257–265, 1984.
Paramonov, M., Grönholm, T., and Virkkula, A.: Below-cloud scavenging of aerosol particles by snow at an urban site in Finland, Boreal Environment Research , 16304 - 320, 10.60910/xjh7-9m7h, 2011.
Párraga, J., Martín-García, J. M., Delgado, G., Molinero-García, A., Cervera-Mata, A., Guerra, I., Fernández-González, M. V., Martín-Rodríguez, F. J., Lyamani, H., Casquero-Vera, J. A., Valenzuela, A., Olmo, F. J., and Delgado, R.: Intrusions of dust and iberulites in Granada basin (Southern Iberian Peninsula). Genesis and formation of atmospheric iberulites, Atmospheric Research, 248, 10.1016/j.atmosres.2020.105260, 2021.
Pouchou, J. L. and Pichoir, F.: PAP ø(pZ) procedure for improved quantitative microanalysis, in: Microbeam Analysis, edited by: Armstrong, J. T., San Francisco Press, 103–106, 1985.
Proestakis, E., Papachristopoulou, K., Georgiou, T., Chatoutsidou, S. E., Lazaridis, M., Gkikas, A., Fountoulakis, I., Tsikoudi, I., Petrakis, M. P., and Amiridis, V.: Atmospheric dust and air quality over large-cities and megacities of the world, Atmospheric Chemistry and Physics, 25, 14777–14823, 10.5194/acp-25-14777-2025, 2025.
Rautela, K. S., Singh, S., and Goyal, M. K.: Characterizing the spatio-temporal distribution, detection, and prediction of aerosol atmospheric rivers on a global scale, J Environ Manage, 351, 119675, 10.1016/j.jenvman.2023.119675, 2024.

Deleted: ¶

Deleted: 6

Deleted: fin6

Deleted: ø

Deleted: ø

Formatted: Font: (Default) Times New Roman, Not Bold

Rolph, G., Stein, A., and Stunder, B.: Real-time Environmental Applications and Display sYstem: READY, Environmental Modelling and Software, 95, 210–228, 10.1016/j.envsoft.2017.06.025, 2017.

Santachiara, G., Prodi, F., Belosi, F., and Nicosia, A.: A Review of Thermo- and Diffusio-Phoresis in the Atmospheric Aerosol Scavenging Process. Part 2: Ice Crystal and Snow Scavenging, Atmospheric and Climate Sciences, 13, 466–477, 10.4236/acs.2023.134026, 2023.

Santos, D., Maurício, A. C., Sencadas, V., Santos, J. D., Fernandes, M. H., and Gomes, P. S.: Spray Drying: An Overview, in: Biomaterials - Physics and Chemistry - New Edition, InTech, 2018.

Schepanski, K., Tegen, I., Todd, M. C., Heinold, B., Bönisch, G., Laurent, B., and Macke, A.: Meteorological processes forcing Saharan dust emission inferred from MSG-SEVIRI observations of subdaily dust source activation and numerical models, Journal of Geophysical Research: Atmospheres, 114, 10.1029/2008jd010325, 2009.

Scheuvens, D., Schütz, L., Kandler, K., Ebert, M., and Weinbruch, S.: Bulk composition of northern African dust and its source sediments - A compilation, 2013.

Schmetz, J., Pili, P., Tjemkes, S., Just, D., Kerkmann, J., Rota, S., and Ratier, A.: An Introduction to Meteosat Second Generation (MSG), Bulletin of the American Meteorological Society, 83, 977–992, 10.1175/BAMS-83-7-Schmetz-2, 2002.

Schwikowski, M., Seibert, P., Baltensperger, U., and Gaggeler, H. W.: A study of an outstanding Saharan dust event at the high-alpine site Jungfraujoch, Switzerland, Atmospheric Environment, 29, 1829–1842, 10.1016/1352-2310(95)00060-c, 1995.

Sokolik, I. N.: The spectral radiative signature of wind-blown mineral dust: Implications for remote sensing in the thermal IR region, Geophysical Research Letters, 29, 10.1029/2002gl015910, 2002.

Stringham, G. E., Simons, D. B., and Guy, H. P.: The behavior of large particles falling in quiescent liquids, 10.3133/pp562C, 1969.

Tagliavini, G., McCorquodale, M., Westbrook, C., Corso, P., Krol, Q., Holzner, M., Tagliavini, G., McCorquodale, M., Westbrook, C., Corso, P., and Krol, Q.: Drag coefficient prediction of complex-shaped snow particles falling in air beyond the Stokes regime Rights / license: Creative Commons Attribution-NonCommercial-NoDerivatives 4.0 International International Journal of Multiphase Flow Drag coefficient prediction of complex-shaped snow particles falling in air beyond the Stokes regime, International Journal of Multiphase Flow, 140, 103652, 10.3929/ethz-b-000480012, 2021.

Tan, F., Zhang, H., Xia, K., Jing, B., Li, X., Tong, S., and Ge, M.: Hygroscopic behavior and aerosol chemistry of atmospheric particles containing organic acids and inorganic salts, npj Climate and Atmospheric Science, 7, 10.1038/s41612-024-00752-9, 2024.

Tobias, A., Karanasiou, A., Amato, F., Roqué, M., and Querol, X.: Health effects of desert dust and sand storms: A systematic review and meta-analysis protocol, 2019.

UNCCD: Sand and Dust Storms Compendium Bonn, 2022.

Velasco-Merino, C., Mateos, D., Toledano, C., Prospero, J. M., Molinie, J., Euphrasie-Clotilde, L., González, R., Cachorro, V. E., Calle, A., and de Frutos, A. M.: Impact of long-range transport over the Atlantic Ocean on Saharan dust optical and microphysical properties based on AERONET data, Atmospheric Chemistry and Physics, 18, 9411–9424, 10.5194/acp-18-9411-2018, 2018.

Wang, Q., Gu, J., and Wang, X.: The impact of Sahara dust on air quality and public health in European countries, Atmospheric Environment, 241, 10.1016/j.atmosenv.2020.117771, 2020.

Weinbruch, S., Wentzel, M., Kluckner, M., Hoffmann, P., and Ortner, H. M.: Mikrochimica Acta Characterization of Individual Atmospheric Particles by Element Mapping in Electron Probe Microanalysis*, 137–141, 1997.

Weinzierl, B., Sauer, D., Esselborn, M., Petzold, A., Veira, A., Rose, M., Mund, S., Wirth, M., Ansmann, A., Tesche, M., Gross, S., and Freudenthaler, V.: Microphysical and optical properties of dust and tropical biomass burning aerosol layers in the Cape Verde region—an overview of the airborne in situ and lidar measurements during SAMUM-2, Tellus B: Chemical and Physical Meteorology, 63, 10.1111/j.1600-0889.2011.00566.x, 2011.

Weinzierl, B., Ansmann, A., Prospero, J. M., Althausen, D., Benker, N., Chouza, F., Dollner, M., Farrell, D., Fomba, W. K., Freudenthaler, V., Gasteiger, J., Groß, S., Haarig, M., Heinold, B., Kandler, K., Kristensen, T. B., Mayol-Bracero, O. L., Müller, T., Reitebuch, O., Sauer, D., Schäfler, A., Schepanski, K., Spanu, A., Tegen, I., Toledano, C., and Walser, A.: The

Formatted: Space After: 0 pt, No bullets or numbering

Formatted: No bullets or numbering

Saharan Aerosol Long-Range Transport and Aerosol–Cloud-Interaction Experiment: Overview and Selected Highlights, Bulletin of the American Meteorological Society, 98, 1427–1451, 10.1175/bams-d-15-00142.1, 2017.

Wiedensohler, A., Birmili, W., Nowak, A., Sonntag, A., Weinhold, K., Merkel, M., Wehner, B., Tuch, T., Pfeifer, S., Fiebig, M., Fjäraa, A. M., Asmi, E., Sellegri, K., Depuy, R., Venzac, H., Villani, P., Laj, P., Aalto, P., Ogren, J. A., Swietlicki, E., Williams, P., Roldin, P., Quincey, P., Hüglin, C., Fierz-Schmidhauser, R., Gysel, M., Weingartner, E., Riccobono, F., Santos, S., Grüning, C., Faloon, K., Beddows, D., Harrison, R., Monahan, C., Jennings, S. G., O'Dowd, C. D., Marinoni, A., Horn, H. G., Keck, L., Jiang, J., Scheckman, J., McMurry, P. H., Deng, Z., Zhao, C. S., Moerman, M., Henzing, B., de Leeuw, G., Löschau, G., and Bastian, S.: Mobility particle size spectrometers: harmonization of technical standards and data structure to facilitate high quality long-term observations of atmospheric particle number size distributions, Atmospheric Measurement Techniques, 5, 657–685, 10.5194/amt-5-657-2012, 2012.